PAPER

Tunable offset locking in a Ξ system: an experimental study on the rubidium atom

Phys. Scr. **88** (2013) 065301 (9pp) doi:10.1088/0031-8949/88/06/065301

Tunable offset locking in a Ξ system: an experimental study on the rubidium atom

Md Sabir Ali, Ayan Ray and Alok Chakrabarti

Radioactive Ion Beam Facility Group Variable Energy Cyclotron Center, 1/AF, Bidhan Nagar, Kolkata 700 064, India

E-mail: sabirbarc@gmail.com

Received 2 March 2013
Accepted for publication 9 October 2013
Published 7 November 2013
Online at stacks.iop.org/PhysScr/88/065301

Abstract

In this report, we present an experimental investigation on atomic frequency offset locking (AFOL) of a laser under ladder (Ξ) level coupling scheme. The $5S_{1/2} \rightarrow 5P_{3/2} \rightarrow 5D_{5/2}$ two-photon transition manifold of the rubidium (Rb) atom is chosen to demonstrate the performance of stabilization scheme in terms of frequency stability and tunability. The coherent pump–probe spectroscopy performed on the $5S \rightarrow 5P \rightarrow 5D$ levels results in signatures of two-photon absorption (TPA) and electromagnetically induced transparency (EIT). Here the pump laser is locked to the fringe of a scanning Fabry–Perot interferometer with the help of frequency modulation spectroscopy. The probe laser is subsequently stabilized on the resulting EIT (TPA) signals. It is found that the probe laser attains relative frequency stability $\sigma(2, \tau) \sim 1.4 \times 10^{-12} (2.0 \times 10^{-12})$ as a square root of Allan variance calculated from the frequency noise power density $S_{\Delta\nu}(f)$ under closed-loop condition. Further, the current locking scheme has wide tuning range {Doppler width of $5S_{1/2}(F = 2 \rightarrow 5P_{3/2}(F')$ transition manifold. This particular tunable AFOL (TAFOL) scheme can provide large tuning range without compromising the frequency stability and such implementation of TAFOL may open new opportunities in research areas like metrology, ultra precision coherent spectroscopy, etc.

PACS numbers: 32.80.Xx, 32.80.Qk, 42.50.Ar, 32.70.Jz

(Some figures may appear in colour only in the online journal)

1. Introduction

Coherent pump–probe spectroscopy [1] has received great attention in the last couple of decades due to the advent of spectroscopic features such as coherent population trapping [1], electromagnetically induced transparency (EIT) [2], electromagnetically induced absorption [3], etc. Among them the EIT has attracted much attention due to its application in versatile fields such as an atomic clock [4], ultra-precision magnetometry [5], slowing down of light [6], AFOL [7–9], etc. It may be noted here that in most of the above-mentioned applications, EIT is realized in a Λ system. This is because EIT in a Λ system is characterized by a zero coherence dephasing rate [10] and is realizable even with a single laser by generating side bands. In the case of AFOL, the EIT signal with sub-natural linewidth obtained through Λ level coupling scheme has been used to exercise offset locking. However, the tunability of AFOL under Λ system is limited because it is difficult to find suitable ultra-narrow EIT signal at will throughout the scanning range of the probe laser. One of the alternative methods may be using the Autler–Townes (AT) doublet as frequency discriminator [11] where the issue of tunability may be resolved. But once again, it is difficult to obtain a workable narrow AT signal at will, which is often observed to have a relatively larger linewidth compared to EIT signal. So a tradeoff exists where the higher tuning range of locking scheme is accompanied with degraded frequency stability.

Optimization of TAFOL, where the question of tradeoff may be addressed more positively compared to the Λ scheme compels us to look into the Ξ system, which has the second best coherent dephasing rate [10]. Earlier work by Jin *et al* [12] has clearly shown that Ξ system spectroscopy reveals the hyperfine structure of excited state in the form of TPA. Other than TPA, which is anyway an obvious outcome, the EIT (result of quantum interference)

can also be obtained depending on the Rabi frequency of the pump laser. It may be noted that in the absence of collisional dephasing, the linewidth of EIT (TPA) is mostly limited by decay rates involved [13]. So the linewidths of EIT and TPA are considerably narrow and can serve as precision frequency reference. Further, the sensitivity of EIT (TPA) signal towards pump frequency detuning is profound, which may help in the realization of TAFOL. The principal difference between the EIT observed in the case of a Λ or a Ξ system is in the appearance of background. While under probe frequency scan, the EIT is observed on a one-photon absorption background [9] for the Λ scheme; the same is observed with a two-photon absorption background for the later-level coupling. This may be clarified from the recent experimental studies by Moon *et al* while re-exploring the Ξ level scheme in connection with double resonance optical pumping (DROP) [14, 15].

There exist earlier works [16, 17] where frequency stabilization of laser is carried out through coherent spectroscopy in a Ξ system. In all these cases, the probe is locked to the saturation absorption spectroscopy (SAS) signal and the pump laser is stabilized to the excited state spectrum (TPA/EIT). However, this situation leaves two issues open: (i) whether the frequency stability of such a coupled laser system is determined by SAS locking and (ii) frequency tunability. The first part is intimately related to the interrelation among SAS, TPA and EIT signals whereas the second part is more related to the extraction of a suitable discriminator signal within the scanning range of the laser. The issue of tunability was not clearly addressed in the earlier reports. This is because suitable SAS locking of probe laser can only be done at discrete points, i.e. the tuning range is small and discontinuous. Further, in a conventional Ξ scheme, where the probe Rabi frequency is much less than the pump one, it is an open issue to explore the degree of coherence-assisted modulation transfer (to be used for frequency modulation spectroscopy (FMS) and locking) in the pump–probe medium.

To address these issues and further to exercise a suitable TAFOL scheme, we have enslaved the pump laser to a Fabry–Perot interferometer (FPI) cavity, thus making the lock point independent of spectroscopic reference and easily tunable. We offset locked the probe laser at different positions using TPA/EIT signals and compared them with the pump laser stability. For FMS, we used only pump modulation. The process of coherence-assisted modulation transfer enables subsequent FMS and frequency locking of probe. To elucidate the situation further, we present a simplistic theoretical model based on our earlier work [18]. We believe that our scheme of TAFOL may find its application in an environment where almost continuous tuning of lock point is required. Also, the current study will help in addressing the issue of limit of frequency stability in a Ξ system. Moreover, the scheme of frequency locking may be successfully used for frequency stabilization in multistep photon–ion interaction processes.

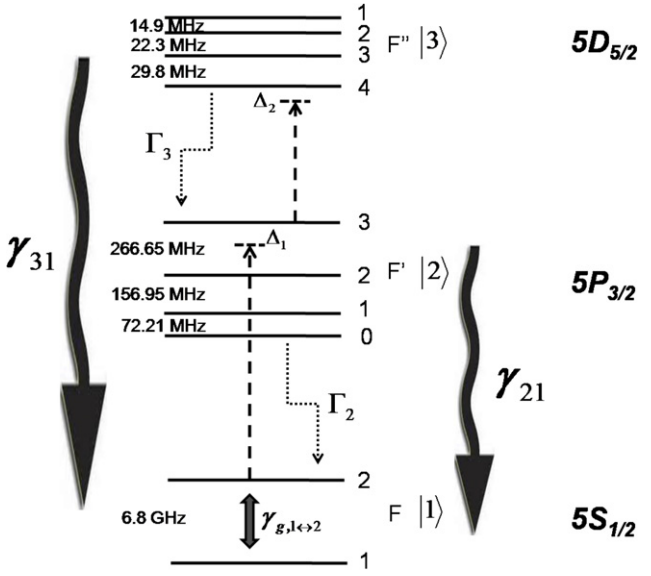

Figure 1. Level scheme in $5S_{1/2} \rightarrow 5P_{3/2}(D_2) \rightarrow 5D_{5/2}$ transition of rubidium atom (^{87}Rb), where the levels relevant for two-photon spectroscopy are denoted by $|1\rangle$, $|2\rangle$ and $|3\rangle$. The probe (pump) laser frequency, detuning and Rabi frequency are ω_1 (ω_2), $\Delta_1(\Delta_2)$ and $\Omega_1(\Omega_2)$, respectively. Dephasing between ground state ($|1\rangle$) hyperfine components ($F = 2, 1$) is $\gamma_{g,1\leftrightarrow2}$. Spontaneous decay rate from $|j\rangle$ is Γ_j. Here $\Gamma_3 = 0.97$ MHz, $\Gamma_2 = 6.066$ MHz, $\Gamma_1 = 0$ are the natural linewidths and $\gamma_{g,1\leftrightarrow2}$ is governed by the transit time broadening (for a room temperature vapour cell without buffer gas). The coherent dephasing rate between $|j\rangle$ and $|i\rangle$ is γ_{ji} (curly arrows) $\approx (\Gamma_j + \Gamma_i)/2$. The two-photon resonance condition is $\Delta_1 + \Delta_2 \approx 0$ where $\Delta_1(\Delta_2)$ are the same as [13].

2. The coherently driven Ξ system and modulation transfer

The level scheme (sample: ^{87}Rb atom) used in our work is shown in figure 1, where a weak probe of frequency ω_1 is tuned in the vicinity of $|1\rangle \rightarrow |2\rangle$ ($5S_{1/2}F = 2 \rightarrow 5P_{3/2}F' = 3, 2, 1$) transition and the strong pump laser of frequency ω_2 dresses the transition $|2\rangle \rightarrow |3\rangle$ ($5P_{3/2}F' \rightarrow 5D_{5/2}F''$). Jin *et al* [12] investigated pump–probe spectroscopy in a realistic Ξ system and their study is based on an earlier work by Banacloche *et al* [13]. Susceptibility (χ) of such a system can be written as

$$\chi(\mathrm{v})\,\mathrm{dv} = \frac{4\mathrm{i}\hbar\Omega_1^2/\varepsilon_0}{\gamma_{21} - \mathrm{i}\Delta_1 - \mathrm{i}\frac{\omega_1}{c}\mathrm{v} + \frac{\Omega_2^2}{4(\sum_{j=1}^{3} A_j)}\left[A_1\{\gamma_{31} - \mathrm{i}(\Delta_1+\Delta_2+\delta_1)\}^{-1} + A_2\{\gamma_{31} - \mathrm{i}(\Delta_1+\Delta_2+\delta_2)\}^{-1} + A_3\{\gamma_{31} - \mathrm{i}(\Delta_1+\Delta_2+\delta_3)\}^{-1}\right]} N(\mathrm{v})\,\mathrm{dv}, \tag{1}$$

where $\Delta_1 = \omega_1 - \omega_{21}$ ($\Delta_2 = \omega_2 - \omega_{32}$) and Ω_1 (Ω_2) are detuning and Rabi frequency of probe (pump) laser, γ_{ij} is the coherence decay rate for $|i\rangle \rightarrow |j\rangle$ transition and $N(\mathrm{v})$ is the Maxwell–Boltzmann velocity distribution of the Doppler broadened ($\Delta\omega_D$) atomic system. The probe

laser absorption coefficient $\{\rho_{21} \infty \mathrm{Im}(\chi)\}$ contains all the necessary dependence of the probe absorption on the pump laser parameters. However, only the lowest-order contribution from probe laser is taken into account as $\Omega_2 \gg \Omega_1$ [13] is the situation. We consider the specific case of the ^{87}Rb atom where $(\omega_2 - \omega_1)/\omega_0 \ll 1$; ω_0 is the nominal frequency of the atomic transition. Here A_j is the line strength of $F_k' \rightarrow F''$ second excited state hyperfine transitions from kth hyperfine component of first excited state. Also, δ_j denotes the jth energy gap between F'' hyperfine levels as measured from $F'' = 4$ position. The $\rho_{21}(\omega_1) \sim \Delta_1$ plot is shown in figure 2(a). For the ^{87}Rb, the relative estimation of A_j can be experimentally obtained from TPA signals (see the caption of figure 2 and the related text for details).

In the case of resonant pump–probe coupling ($F = 2 \rightarrow F' = 3 \rightarrow F'' = 4$), the zero velocity group of atoms, which are simultaneously at resonance with pump (probe) lasers, will get transferred to $|3\rangle$. Similarly, we can consider the situations under $F' = 3 \rightarrow F'' = 3 (= 2)$ pump transitions. In all these cases (i.e. $\Delta_2 < \Delta\omega_\mathrm{D}$), the TPA will be demonstrated through sharp and discrete transparency (reduced absorption) windows imprinted on the one-photon absorption background. In figure 2(a), three sharp TPA features, mimicking the hyperfine structure $F'(= 3) \rightarrow F''(= 4, 3, 2)$ of $5D_{5/2}$ state, appear as a consequence of $\Delta E_{F' \rightarrow F''} \ll \Delta E_{F \rightarrow F'}$, i.e. ω_2 may be considered at exact/near exact resonance for all values of ω_1. The TPAs appear as transparencies on the one-photon probe absorption ($F = 2 \rightarrow F'$) background. Considering the 'generalized pump Rabi frequency' $\overline{\Omega_2} = \sqrt{\Omega_2^2 + \{\Delta_2(v)\}^2}$ [19], which essentially completes the ensuing two-photon coupling of $F = 2 \rightarrow F' = 3 \rightarrow F'' = 4, 3, 2$, gives rise to the TPAs (cf figure 2(a)). However, equation (1) alone cannot fully explain the EIT-based transparency as it is always accompanied by strong TPA.

To explain the presence of EIT within the TPA signal, one may consider the generalized two-photon resonance condition, i.e. $\Delta_1 + \Delta_2 \approx 0 \approx (\omega_1 - \omega_{21}) + (\omega_2 - \omega_{32}) = (\omega_1 - \vec{k}_1 \cdot \vec{v}) + (\omega_2 - \vec{k}_2 \cdot \vec{v})$, where it is $\vec{k}_1 \approx -\vec{k}_2$ in our case. For each velocity group of atoms, the AT splitting occurs and overall velocity averaging of all these AT components produces two discrete absorption spectra accounting for the AT effect (like the Λ system [20]). The dephasing (γ_{31}, decay between dipole-forbidden transition levels) actually determines the location of maximum transparency between these two absorption peaks. In case of $\mathrm{Lim}_{\gamma_{31} \rightarrow 0}$ and $\Delta_1 \approx \Delta_2 \approx 0$, maximum transparency is observed and coincides with the position of EIT. For finite value of γ_{31}, the EIT becomes weaker, the transparency window becomes wider and shifts from the position of EIT. The EIT itself appears as a consequence of formation of a so-called 'Dark State' due to the dressing of bare atomic levels [21]. As a result, the absorbing medium becomes transparent to the probe laser resulting into EIT (two-photon coherence) signal observed on TPA (two-photon absorption) background.

We present here an outline of the process of modulation transfer in a Ξ system by following a rather simplified picture presented earlier [22] for Λ system. In analogy with Λ scheme, where $(\Omega_2^2/\Gamma) \gg \gamma_{\mathrm{dipole-forbidden}}$ is necessary for the observation of EIT, we may consider $(\Omega_2^2/4\gamma_{21}) \gg \gamma_{31}$ [13] condition playing the same role in the case of Ξ system.

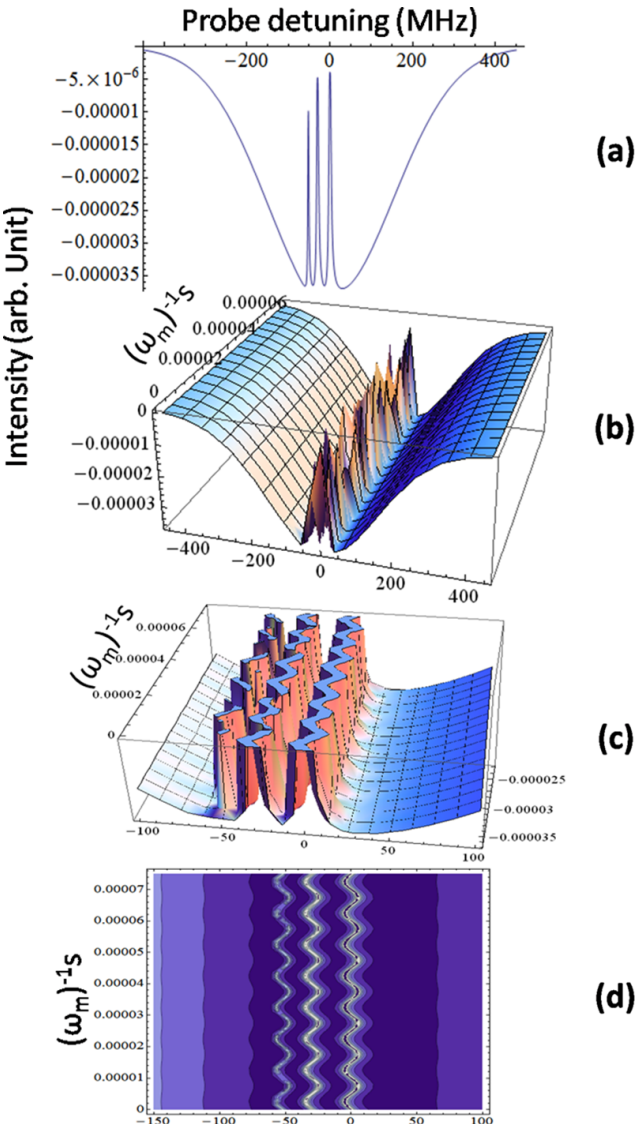

Figure 2. Theoretical simulation of modulation transfer in the Ξ system of figure 1 with $\Delta_2 \rightarrow \Delta_0 + A \sin \omega_\mathrm{m} t$ substituted in equation (1). (a) Plot of Doppler-averaged probe absorption spectrum $\rho_{21}(\omega_1) \sim \Delta_1$, (b) Doppler-averaged probe absorption spectrum under pump frequency modulation, showing modulation transfer around transparency window. The transfer is zero elsewhere in the spectrum. (c) A closer snapshot of the same reveals modulation transfer on three transparency peaks. The transparency includes effects of both TPA and EIT. Contour plot (d) reveals the same result in a more clarified manner. Here modulation frequency $\omega_\mathrm{m} \approx 100$ kHz is wilfully chosen to clearly visualize the numerical simulation results. Since the general criterion behind additive inclusion of modulation is $\omega_\mathrm{m}^{-1} \ll \{(\Omega_2^2/\gamma_{21})^{-1}, \gamma_{31}^{-1}\}$, the same result is obtained with experimental parameter $\omega_\mathrm{m} \approx 5$ kHz.

Thus, the principal physical mechanisms associated with the Ξ system are of timescales: $(\Omega_2^2/\gamma_{21})^{-1}$, γ_{31}^{-1} (cf caption of figure 2). We consider FM by introducing $\Delta_2 \rightarrow \Delta_0 + A \sin \omega_\mathrm{m} t$ in equation (1); Δ_0 is the nominal detuning and ω_m is the modulation frequency. For demonstration, we use here slow modulation frequency (on resonance condition), i.e. $\omega_\mathrm{m} = 100\,\mathrm{kHz} (\Delta_0 \approx 0)$ (see figure 2(b)). As the hyperfine components of the 5D states are too closely spaced, the propagation of single-colour frequency for all the three peaks, where Doppler averaging is considered, are not distinct in figure 2(b). A closer snapshot presented in figure 2(c) and

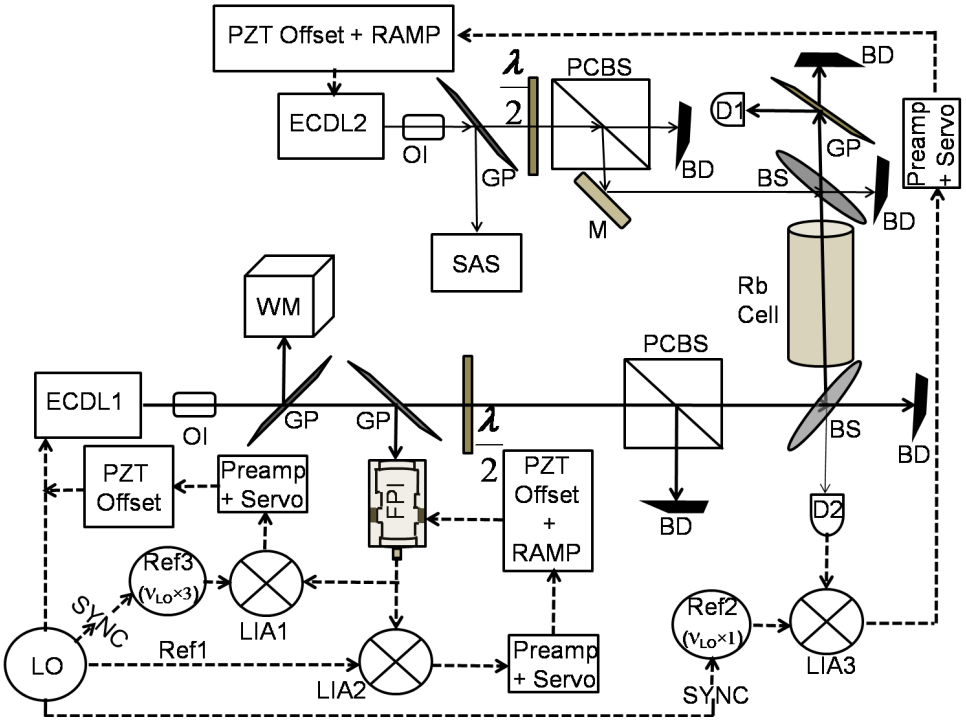

Figure 3. Schematic diagram of the experimental arrangement., M: mirror; BS: beam splitter; PCBS: polarizing cube beam splitter; OI: optical isolator; BD: beam dump; D: photodetector; $\lambda/2$: half waveplate; FPI: Fabry–Perot interferometer; WM: wavemeter; LO: local (mother) oscillator; Ref: reference oscillator; GP: glass plate; and SAS: saturation absorption spectroscopy. Preamp + Servo combo unit is used for frequency stabilization of the laser. The 'Ref' oscillators are synchronized by the 'mother'. For synchronization, 'star' configuration is used instead of 'daisy chain' to minimize phase skew.

the associated contour plot (cf figure 2(d)) clearly reveals the presence of modulation on the TPA signals. The additive inclusion of sinusoidal frequency is appropriate in view of the fact that $\omega_m^{-1} \ll \{(\Omega_2^2/\gamma_{21})^{-1}, \gamma_{31}^{-1}\}$, i.e. the duty cycle of modulation is so slow that it actually enslaves other processes responsible for building up the coherence. One may consider this external perturbation as a smooth flow, where, in principle, the dynamic evolution of the system can be described in the timescale of ω_m^{-1}.

3. Experiment

The experimental schematic is shown in figure 3 where two lasers external cavity diode laser (ECDL)1 andECDL2 are used as probe (pump) with Rabi frequencies $\Omega_1 \sim 9$ MHz ($\Omega_2 \sim 70$ MHz) [23]. Both beams are linearly polarized. A small part of the probe beam is used in a saturation absorption spectroscopy (SAS) setup to reveal the hyperfine structure of $F = 2 \rightarrow F' = 3, 2, 1$ of Rb D_2 transition and it helps us during the calibration of the probe absorption spectrum.

The pump laser is used in a propagating configuration counter to the probe beam. This particular geometry helps in largely eliminating the first-order Doppler broadening as $\omega_1 \approx \omega_2$. In the first part of the experiment, the probe laser is directly side-locked to $5S_{1/2}(F = 2) \rightarrow 5P_{3/2}(F' = 3)$ component of the SAS. The pump laser frequency is scanned across the $5P_{3/2} \rightarrow 5D_{5/2}$ transition manifold and is also monitored by using a scanning FPI. Since $\Omega_1 \ll \Omega_2$ and $\Delta_1 \approx 0$, a very limited number of atoms are pumped to 5P state by the probe laser. As a result, the TPA signals appear on a flat background under the scan of ω_2 (figure 4). The

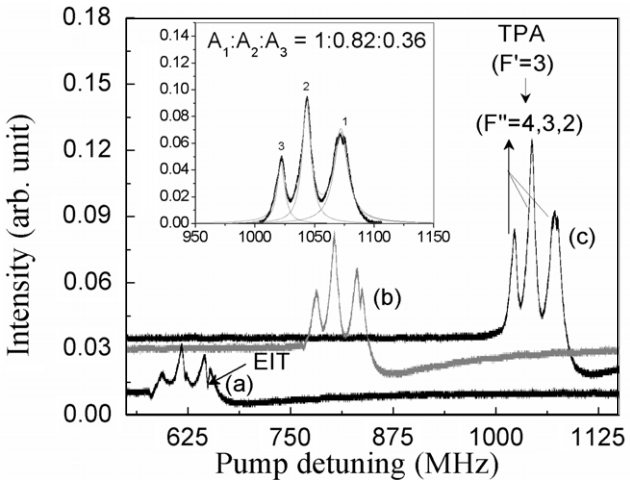

Figure 4. The probe absorption spectrum as a function of pump frequency scan. Here the probe laser is side-locked to amplified signals of (a) crossover transition between $5S_{1/2}(F = 2) \rightarrow 5P_{3/2}(F' = 2, 1)$, (b) crossover transition between $5S_{1/2}(F = 2) \rightarrow 5P_{3/2}(F' = 3, 1)$ and (c) closed transition $5S_{1/2}(F = 2) \rightarrow 5P_{3/2}(F' = 3)$. Rabi frequency combination $\Omega_2(\Omega_1)$ is 70 MHz(9 MHz). Here (a) shows (prominent EIT+ reduced TPA) feature whereas (strong TPA + very weak EIT) is seen in (c). Under pump scan, the *X*-axis of the spectrum is calibrated with the help of simultaneous recording of FPI fringes. The inset shows the result of fitting of TPAs (cf plot (c)) to evaluate their relative line strengths. The result is used in equation (1) for numerical simulation (cf figure 2(a)).

relative line strengths $(A_1 : A_2 : A_3 \approx 1.0 : 0.82 : 0.36)$ of TPA signals are estimated by considering the fitted area under the respective curve and this is utilized in a simulation based

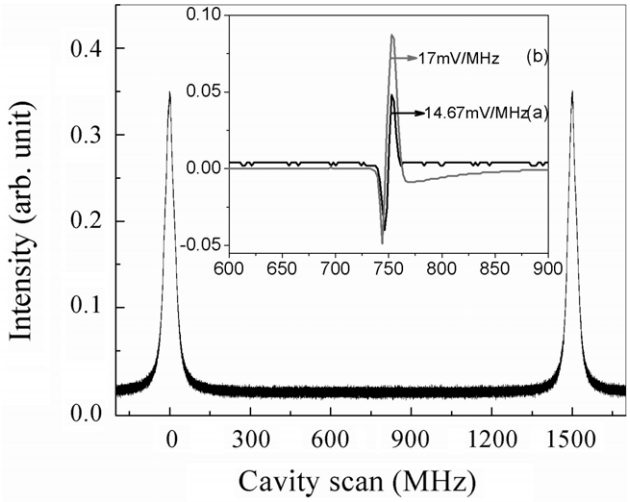

Figure 5. Recording of fringes (F.S.R 1.5 GHz, FWHM ∼ 5.3 MHz) with the scanning of FPI (Thorlabs SA-200-5B). The RAMP and piezo offset of the FPI driver are adjusted to zoom on one particular fringe matching the pump frequency position (selected for two-photon atom-field interaction). Inset shows (a) 1f output from LIA2 (cf figure 3) and (b) 3f output from LIA1 after the frequency modulation to pump laser is switched on. The slopes for 1f (3f) are 14.67(17) mV MHz^{-1} and are used for frequency stabilization.

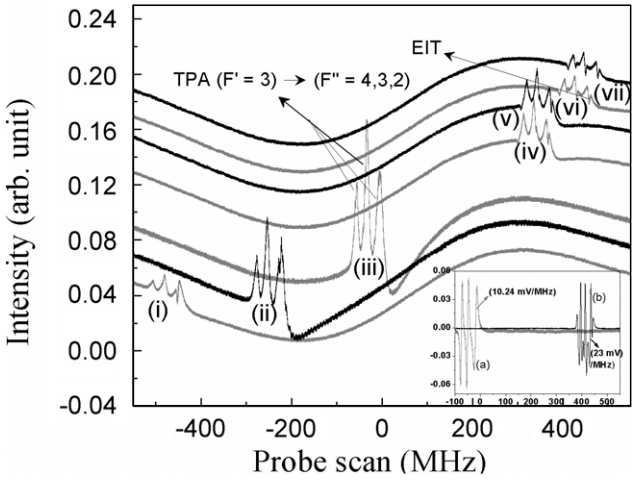

Figure 6. Recording of probe absorption spectra (i) → (vii) as a function of probe detuning. Here $\Omega_1(\Omega_2)$ are kept the same as in figure 4 (see caption). The pump laser is static (free running) at different frequency positions. Initially, simultaneous recordings of probe absorption and probe SAS spectra (used for calibration) are monitored on an oscilloscope. The piezo offset of the pump laser is adjusted to bring the two-photon spectrum matching exactly on the same position of closed transition $5S_{1/2}(F = 2) \rightarrow 5P_{3/2}(F' = 3)$ for plot (iii). Other positions, namely (i), (ii), (iv) → (vii) of the pump frequency are adjusted by monitoring the instantaneous readout on the wavemeter. It is seen in plot (vii) that asymmetric EIT signals appear within all TPA components, indicating strong influence by AT components (contributed through different velocity groups of atoms). Inset shows (a) 1f signal of TPA and (b) the same of EIT when (a) TPA originates from $F = 2 \rightarrow F' = 3 \rightarrow F''$ coupling and (b) EIT appears due to $|\Delta_2| = 450$ MHz from $F' = 3 \rightarrow F'' = 4$ condition while probe is scanning over $F = 2 \rightarrow F'$ manifold. The slopes of TPA(EIT) are 10.24 mV MHz^{-1} (23 mV MHz^{-1}). Here (a) and (b) correspond to the probe absorption spectra (iii) and (vi).

on equation (1). Note here that this estimate includes the effect of individual laser linewidth ($\Delta\nu$) too.

To demonstrate offset locking of probe laser (∼780 nm), we need to stabilize the pump laser at a frequency matching $5P_{3/2} \rightarrow 5D_{5/2}$ transition. This is an odd wavelength (∼776 nm) where spectroscopic transition with a significant population in the lower state is unavailable. Also, for tunable offset locking, it is desired to tune the lock point of the pump frequency over a wide zone. These two stringent conditions compel us to explore the possibility of using a scanning optical cavity reference (here FPI is used). To choose the exact frequency of the pump laser for the observation of TPA, we scan the probe laser $5S_{1/2}(F = 2) \rightarrow 5P_{3/2}(F')$ for a free running pump laser. After the TPA signals are seen on the oscilloscope, the piezo offset of pump laser is fine-tuned to shift the TPAs to a desired position. Once this is accomplished, the FPI is scanned with a RAMP and fringes are observed on a separate oscilloscope (see figure 5). The piezo offset and RAMP are further adjusted to zoom on one fringe, which corresponds to the FPI cavity discriminator. At this stage, a small current modulation ($\Delta\nu_m < 1$ MHz) is applied to the pump laser for FMS. By using phase sensitive detection (PSD), 1f spectrum of the fringe is extracted (see inset of figure 5). Using another separate but phase-locked PSD (see figure 3 and caption), we further extract the 3f spectrum of the fringe discriminator. The 1f signal reveals the deviation of the FPI transmission from its maximum value and the respective servo loop is used to provide electrical feedback to the piezo transducer (PZT) of FPI for stabilization.

Once the FPI is stabilized to zero crossing (maximum transmission) point of 1f discriminator (cf inset of figure 5), the error signal obtained at lock-in amplifier (LIA)1 (3f discriminator output, see figure 3) detects consequent pump laser frequency fluctuations from the FPI lock point. Thus by closing the 3f-signal-based servo loop, we can stabilize the laser to the FPI cavity fringe. As FPI fringes are easy to find at any wavelength within the pass band of the cavity, the locking scheme is also easy to implement and can be smoothly tuned throughout a wide region. The tuning range can cover the entire region of two-photon interaction (i.e. $\Delta\omega_D$ of $5S_{1/2} \rightarrow 5P_{3/2}$ transition and its immediate neighbourhood; see figure 6). In effect, the TPA/EIT signature can be shifted continuously within or around the linewidth of probe transmission; thus offering a wide tuning of offset reference.

The frequency modulation introduced to the pump laser gets transferred to the probe due to coherent crosstalk. After slaving the pump laser to the FPI, in principle one can extract the 1f discriminator signal of the probe laser transmission (see inset of figure 6) by exploiting the modulation transfer. Here, another PSD (cf figure 3), which is also phase-locked to the mother oscillator, is used to extract the 1f discriminator signal of respective TPA/EIT signal based on the combination of Δ_2, Ω_2. Afterwards, the servo loop is closed to stabilize the probe laser on the TPA/EIT reference by using electrical feedback. Once the FPI and the pump and probe lasers are stabilized, the error signals are recorded. Fast Four transformation (FFT) is carried out on the recorded error signal to reveal the frequency noise power spectral density $S_{\Delta\nu}(f)$ (see figure 7). This is further used to numerically

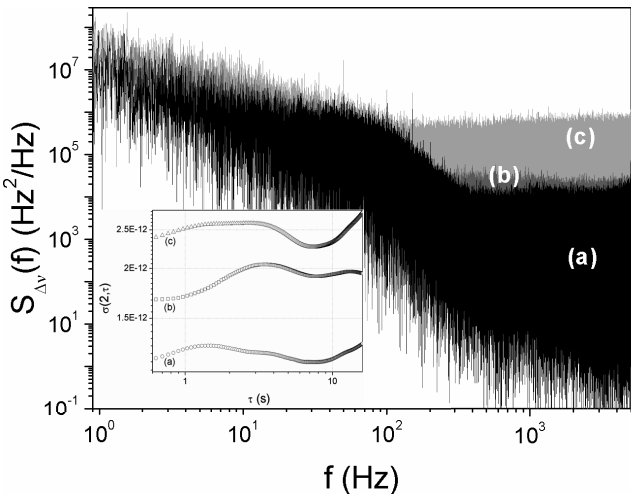

Figure 7. Frequency noise power density ($S_{\Delta\nu}$) versus Fourier frequency (f) plots for (a) probe EIT lock (b) FPI cavity fringe lock of pump and (c) probe TPA lock as calculated from closed-loop error signal using FFT analysis. The plot (a) clearly shows the control bandwidth ~100 Hz where a PI control is used. Inset shows the square root of Allan variance $\{\sigma(2,\tau)\}$ versus integration time (τ)plots for three different frequency stabilization situations. See the text for details.

calculate square root of Allan variance $\sigma(2,\tau)$, which is the indicator of frequency stability (cf inset of figure 7).

4. Results and discussions

The result of the experiment, as shown in figure 4, shows the probe absorption spectra as a function of pump detuning. It can be seen that the TPA and TPA+EIT signals are observed on almost Doppler-free background for a frequency-locked probe laser. As the probe laser frequency is locked at respective SAS signals, ω_1 resonates with small velocity groups of atoms (taking into consideration laser linewidth $\Delta\nu_{\text{laser}}$).These atoms reach the upper state $|3\rangle$ due to the presence of the pump laser. As a result, the usual presence of Doppler background (as seen under probe laser scanning, pump laser fixed) is not observed. It is seen in figure 4(c) that extremely weak EIT feature is present within $F'=3\rightarrow F''=4$ profile (probe laser side-locked to $F=2\rightarrow F'=3$ closed transition), whereas no such signature of EIT is noticed for $F'=3\rightarrow F''=3,2$ components. On the other hand, when the probe laser is locked on the crossover transitions between $F=2\rightarrow F'=3,1$ and $F=2\rightarrow F'=2,1$ hyperfine components, the strength of the TPA is gradually reduced (see figures 4(b) and (a)) and the EIT signals are clearly visible.

We may note here that for TPA, the main decay factor is a combination of $\Gamma_3(0.97\,\text{MHz})$, $\Gamma_2(6.066\,\text{MHz})$ and for EIT, the decoherence part is $\gamma_{31}(\Gamma_3/2\approx 0.5\,\text{MHz})$, $\gamma_{21}(\Gamma_2/2\approx 3.0\,\text{MHz})$ [13]. Also, it is a physical fact that $\Delta E_{F'\rightarrow F''}\ll\Delta E_{F\rightarrow F'}$ (cf figure 1). Hence $F=2\rightarrow F'=3\rightarrow F''$ indicates almost resonant coupling of atoms between $5S_{1/2}\rightarrow 5D_{5/2}$ levels. Other than $F'=3\rightarrow F''=4$ transition, the atoms coupled via $F'=3\rightarrow F''=3,2$ excitation routes can decay back to $F=1$ level, i.e. migrate outside the present Ξ level coupling scheme. This mechanism is known as double resonance optical pumping (DROP) [14, 15] and it is always present with the TPA spectra. It may be noted that both DROP (which is proportional to the TPA probability [15]) and EIT are present under two-photon resonance condition, i.e. $\Delta_1+\Delta_2\approx 0$. However, the decay route $F=2\leftarrow F'=3$ (branching ratio $\eta=1$)$\leftarrow F''=4(\eta=0.74$ [24]) helps in forming a pseudo closed absorption–emission cycle $F=2\leftrightarrow F'=3\leftrightarrow F''=4$, where the probability of losing atoms to $F=1$ level due to the DROP mechanism is minimum. This is why the EIT is noticeable on $F'=3\rightarrow F''=4$ profile, while it is absent on other peaks (cf figure 4(c)).

In case of figures 4(b) and (a), the probe frequency is locked subsequently to the positions of $\omega_{23}-212\,\text{MHz}$ and $\omega_{22}-345\,\text{MHz}$. The detuning ($\Delta_1$) of probe laser is taken into account by considering 'generalized Rabi frequency' $\overline{\Omega}_1=\sqrt{\Omega_1^2+\Delta_1^2}$ [22], which addresses broader velocity group of atoms (less frequency selective compared to $F=2\rightarrow F'=3$ case) and it results into non-resonant two-photon transition $F=2\leftrightarrow F'\leftrightarrow F''$. Average population in $F''=3,2$ levels increases, as well as the probability of decay of atoms to $F=1$ level also increases due to the presence of DROP. Since the probe laser is largely off-resonant to $F=2\rightarrow F'=3$ transition, net supply of atoms to F'' levels is much lower compared to the earlier situation (see figure 4(c)). This results in a relatively weaker DROP as evident in figures 4(a) and (b) compared to the case of closed transition presented in figure 4(c). As a result, the EIT, which is anyway present due to the satisfaction of conditions: (i) $(\Omega_2^2/4\gamma_{21})\gg\gamma_{31}$ and (ii) $\Delta_1+\Delta_2\approx 0$, is prominent.

To have an idea about the relative line strengths of individual $F'=3\rightarrow F''$ component, we estimate the area under the TPAs as recorded in figure 4(c). The ratio (cf inset of figure 4) is used in simulation centred on equation (1). Note here that this part of the experiment is conducted without applying FMS for probe frequency locking; thus the broadening of spectral profile due to modulation is avoided. Also, other possible decay routes, as permitted under selection rule, are present to a small extent due to the leakage of atoms from the $F=2\leftrightarrow F'=3\leftrightarrow F''=4$ absorption–emission cycle to populate the $5S_{1/2}(F=1)$ level; therefore they can reduce absorption. However, this effect is very minimal for a closed transition. In the present case, a room-temperature Rb vapour cell (without buffer gas) is used; hence the dephasing mechanism $\gamma_{g,1\leftrightarrow 2}(F=2\leftrightarrow 1)$ is mainly governed by transit time effect. This process is very slow ($\sim<50\,\text{kHz}$) compared to other relatively faster processes (e.g. optical pumping and decay). Their effects on the atom-field dynamics are averaged many times within the much longer duty cycle of $\gamma_{g,1\leftrightarrow 2}$, thus settling the system into equilibrium.

In the next part of the experiment, we focus on the situation where probe laser is scanned over $F=2\rightarrow F'$ hyperfine levels and the pump laser is kept stationary (free running) at a nominal frequency, $\nu_0\sim 776\,\text{nm}$. The probe absorption spectra (see figure 6) clearly show the evolution of TPA+EIT feature with change in pump detuning. By observing the signals from all photodiodes on the oscilloscope, the pump frequency is fine-tuned to match the position of the TPA/EIT features. The probe SAS spectra are used for calibration purpose. Since the recording is

done within ∼1 s time window, the long-term drift of ω_2 does not affect the resultant spectrum. Apart from the presence of one-photon $F = 2 \rightarrow F'$ absorption background, figure 6(c) is identical to the spectrum of figure 4(c). The piezo offset is adjusted to shift ω_2, which shifts the two-photon feature at various positions (see figure 6). The EIT feature becomes more and more clear with the weakening of DROP due to the departure of pump frequency from the $F = 2 \rightarrow F' = 3 \rightarrow F''$ resonant TPA coupling condition. The asymmetry in EIT signals on TPA background clearly indicates the strong influence of AT splitting of different velocity groups of atoms [19] during probe scan. The probe coupling ($F = 2 \rightarrow F'$) also facilitates 'single resonance optical pumping' where atoms decay back to $F = 1$ level, effectively reducing the absorption. This effect also contributes to reducing absorption as probe frequency is detuned from the closed transition.

The last part of the experiment is conducted in search of tuning of offset reference and extraction of workable discriminator signal. We focus on figure 6, where plots (i) → (vii) show offset tuning of TPA+EIT signals over a range of $\Delta_1 \sim 1$ GHz. The significant difference between the Λ and Ξ systems lies in the fact that the latter presents EIT with sub-natural ($< \Gamma_2$) linewidth almost throughout the $F = 2 \rightarrow F'$ absorption profile (more prominently away from the line centre, i.e. $F = 2 \rightarrow F' = 3$ transition) whereas the Λ scheme can produce the same only at a very limited number of points, especially at the line centre. This offers a unique opportunity where one may find out the sub-natural atomic offset reference, at will, over a wide frequency region. However, to execute such a TAFOL scheme, it is required to precisely lock the pump laser. Here, the pump is locked to an FPI cavity fringe (see figure 5). Note here that $\mathrm{FWHM}_{\mathrm{fringe}} \sim$ 5 MHz, which is considerably less than the overall frequency spacing of the $5D_{5/2}$ $F'' = 4, 3, 2, 1$ ($\delta\nu_{F''} \sim 50$ MHz) and also less than Γ_{TPA}. Hence the FPI fringe locking reference is sufficient to fix the pump laser at the desired frequency for selection of two-photon events (DROP or EIT).

Inset of figure 5 shows (a) 1f and (b) 3f signals of the fringe after modulation to pump laser is switched on. The FPI is locked first to the zero crossing reference of 1f signal, afterwards the pump laser feedback loop is closed to stabilize on the 3f derivative of set point. We employed proportional–integrator (PI) control loop for negative feedback. The open-loop corner frequency (3 dB) of the PI loop is ∼500 Hz, which matches well with the piezo bandwidth. Since the piezo actuator with ECDL is more responsive than the same in an FPI, the 3f signal with relatively higher slope is a suitable choice for the laser stabilization. After slaving the pump to the FPI, we obtain a stable frequency reference ∼776 nm. Once this is accomplished, the FMS of probe scan generates the 1f discriminator of TPA+EIT spectral feature (see inset of figure 6). The probe laser experiences frequency modulation due to coherence-assisted transfer of the same. The probe is subsequently locked on two different discriminators at two different positions: (a) TPA originating from $F = 2 \rightarrow F' = 3 \rightarrow F'' = 4$ coupling and (b) EIT originating due to $|\Delta_2| =$ 450 MHz from $F' = 3 \rightarrow F'' = 4$ condition while probe is scanning over $F = 2 \rightarrow F'$ manifold. The 1f signals ((a) and (b)) in the inset of figure 6 correspond to 1f derivative of the plots (iii) and (vi) in the same.

Before analysing the frequency stability, we focus on the linewidth of TPA (Γ_{TPA} limited by spontaneous decay) [17] and EIT ($\Gamma_{\mathrm{EIT}}(= \gamma_{31} + \Delta\nu_1 + \Delta\nu_2)$ limited by coherence decay rate and $\Delta\nu$) signals. Theoretical values are $\Gamma_{\mathrm{TPA}}(\Gamma_{\mathrm{EIT}}) \approx 8.5(2.1)$ MHz and they match well with the experimental results of 9.01(3.5 MHz (measured from the excursion between the extreme points on the slope of first derivative signal shown in the inset of figure 6). Note here that a part of the linewidth is also contributed by the modulation introduced for FMS. Further, it may be pointed out that $\Gamma_{\mathrm{EIT}} < \Gamma_2$, i.e. of sub-natural width. Furthermore, $\Gamma_{\mathrm{TPA}} \sim \Gamma_2$, i.e. the TPA acts as a discriminator almost equivalent to the least value achievable for Γ_{SAS} for alkali atom [25]. Hence the TAFOL scheme does not pose any serious trade-off between wide tunability and discriminator linewidth. This has happened due to mutual competition between DROP and EIT mechanisms throughout $\Delta\omega_{\mathrm{D}}$ and this subtle point strongly supports the prospective application of Ξ scheme compared to its Λ counterpart for TAFOL.

Before analysing the case of frequency stability of the individual lasers, we present the slopes ($\delta V/\delta\nu$) of the discriminators (see inset of figures 5 and 6), which are as follows: EIT : FPI : TPA ≈ 23 mV : 17 mV : 10.24 mV. After closing the PI loop, the error signal is recorded for each of the discriminator. The recorded error signal is FFT analysed and the resultant data is used for the calculation of square root of Allan variance $\sigma(2, \tau)$ using the equation [26–28]:

$$\sigma^2(2, \tau) = \frac{2}{\nu_0^2} \int_0^\infty S_{\Delta\nu}(f) \frac{\sin^4(\pi f \tau)}{(\pi f \tau)^2} \mathrm{d}f. \qquad (2)$$

Here τ is the integration time and ν_0 is the nominal frequency (3.843×10^{14} Hz). Frequency noise power spectral density $\{S_{\Delta\nu}(f)\}$ versus Fourier frequency (f) data obtained from FFT analysis of error signal (cf figure 7) is used in equation (2). Inset of figure 7 shows the behaviour of $\sigma(2, \tau)$ versus τ for the pump (FPI stabilized) and probe laser subsequently stabilized on EIT/TPA references. It is observed that at $\tau = 10$ s, the EIT (TPA) locked probe laser attains a stability of $\sigma \sim 1.2 \times 10^{-12}(2.35 \times 10^{-12})$ whereas the pump laser shows $\sigma \sim 2.4 \times 10^{-12}$. The above-mentioned method of measuring frequency stability under closed-loop condition does not consider the noise of the discriminator [28] because the error signal is weighted by the servo loop transfer function $H(f)$. In effect, the values of $\sigma(2, \tau)$ calculated earlier predicts the best case of frequency stability [28]. However, despite this limitation, the closed-loop method can effectively explore the relative frequency stability of the laser.

We now focus on the nature of the atomic frequency offset locking referenced to EIT (TPA) resonance w.r.t. the FPI locking. Under relatively shorter averaging timescale ($\tau \approx 0.5 \rightarrow 20$ s; see inset of figure 7), the EIT lock behaves best amongst the three cases, which is expected due to the steeper slope of the EIT discriminator. However, it can be noticed that the EIT lock is superior compared to the stability of the pump. This may be attributed to the fact that in a Ξ system (for $\Delta_1 \approx \Delta_2 \approx 0$), the necessary condition for EIT

is $(\Omega_2^2/\gamma_{21} \gg \gamma_{31})$ [13], which is analogous to $(\Omega^2/\Gamma \gg \gamma_{\text{dipole-forbidden}})$ condition in a Λ system. In effect, for a much reduced value of γ_{31} (here $\gamma_{21} \approx 6.0\gamma_{31}$ for $5S \rightarrow 5P \rightarrow 5D$ coherence), the large value of the factor (Ω_2/γ_{31}) helps in the observation of substantial transparency [13] at the line centre. In analogy with the Λ scheme, we may consider (Ω_2^2/γ_{21}) as the necessary optical pumping (other than DROP) required for setting the EIT coherence. In case of non-resonant EIT (i.e. $\Delta_1 + \Delta_2 \approx 0$ but $\Delta_1 \neq 0 \neq \Delta_2$), the optical pumping $\overline{\Omega_1}^2/\gamma_{21}$ is still strong enough to set up two-photon coherence. It may be seen that in an ideal case, Γ_{EIT} is a function of γ_{31} only; hence Γ_{EIT} is almost immune to the effect of pump frequency fluctuations provided $|\Delta_1 + \Delta_2| \sim \gamma_{31}$ is maintained.

The other issue regarding variation in magnitudes of slopes in the case of EIT and TPA resonances also indicates different degree of modulation transfer. In this connection, we may borrow the conclusions of Brown and Xiao [29] while considering EIT medium in a Λ system. The modulation transfer function $T(\omega_{\text{mod}})$ is a strong function of residual Doppler width (δW_{D}). The higher degree of $T(\omega_{\text{mod}})$ may be due to $\delta W_{\text{D}} \rightarrow 0$ as present in the case of the current Ξ scheme. It is to be noted that the extraction of derivative signal in FMS typically depends on the modulation depth. The steeper slope of EIT clearly exhibits a higher degree of modulation transfer due to EIT-type coherence compared to the TPA.

5. Conclusion

In this work, we explored the prospective application of Ξ system for the purpose of AFOL. It is noticed that the presence of two types of mechanisms—the DROP and the EIT—dominate the probe laser absorption spectrum in a Ξ system. The strength of DROP is proportional to TPA signal. The effect of detuning of pump/probe laser on the TPA(EIT) spectrum is investigated in details. Under the application of external frequency modulation to the pump laser, it is found that the system probe can also experience the modulation transfer due to two-photon coupling. A phenomenological presentation (in line with [18]) of modulation transfer under Ξ level coupling is presented to visualize the physical picture. It is found that modulation transfer is more effective for EIT compared to DROP and it helps in the extraction of 1f signal with steeper slope. The result of subsequent frequency stabilization of probe laser on TPA and EIT reference is also presented. It is found that the EIT-locked laser exhibits better frequency stability in a shorter integration time $\tau = 0.5 \rightarrow 20$ s, resulting into $\sigma(2, \tau) \approx 1.2 \times 10^{-12}$ whereas TPA locking shows 2×10^{-12} relative frequency stability. Further, during the experiment, the pump laser, emitting at $\sim$776 nm, is locked to the cavity fringe of a FPI. Since the two-photon resonance condition for EIT is at $\sim$450 MHz offset from the line centre, the pump laser is accordingly offset locked to match the aforementioned position. The probe laser is stabilized on the two-photon resonance exhibiting the tunability of the offset locking scheme.

In summary, our experimental study helps in creating a tunable offset reference with a 780 nm laser (resonant with Rb D_2 transition), which is continuously tunable over a range of more than 1 GHz (throughout $\Delta\omega_{\text{D}}$ of $5S_{1/2} \rightarrow 5P_{3/2}$ and its immediate neighbourhood). The striking point of the current TAFOL scheme is that we did not really face any stiff trade-off situation between a large tuning range and discriminator linewidth. Unlike TAFOL based on AT signal [11], the current scheme deals with a discriminator linewidth varying within 8.5 MHz(Γ_{TPA}) $\leftrightarrow$ 2.1 MHz(Γ_{EIT}). The value of Γ_{TPA} is almost equivalent to the best case of Γ_{SAS} [25], thereby exhibiting near immunity of offset reference on the tuning range. In effect, this result will be helpful in applications where continuous tunability and precision frequency stability are simultaneously required. Further, it is noteworthy that unlike previous cases [16, 17] where the FM transfer from probe to pump laser is utilized, we considered the reverse situation. Since in a classical two-photon coherence (EIT) experiment, the emphasis is on ac Stark shift, $\Omega_1 \ll \Omega_2$ is always maintained. The implicit meaning is that the coherence is controlled by the pump laser. Indeed, we observed lesser degree of modulation transfer for the probe→pump laser system while particularly experimenting in line with [17]. It requires relatively stronger modulation to produce a workable discriminator, which in due course introduces larger instrumental linewidth. Using costly external modulators may reduce this problem, but on the other hand it introduces further complexity in the experimental schematic.

References

[1] Arimondo E 1996 *Progress in Optics* vol XXXV (Amsterdam: Elsevier) p 257
[2] Boller K J, Imamoglu A and Harris S E 1991 *Phys. Rev. Lett.* **66** 2593
[3] Akulshin A M, Barriero S and Lezamo A 1998 *Phys. Rev.* A **57** 2996
[4] Knappe S, Shah V, Schwindt P D, Hollberg L, Kitching J, Liew L and Moreland J 2004 *Appl. Phys. Lett.* **85** 1460
[5] Stähler M, Knappe S, Affolderbach C, Kemp W and Wynands R 2001 *Eur. Phys. Lett.* **54** 323
[6] Kocharovskaya O, Rostovtsev Y and Scully M O 2001 *Phys. Rev. Lett.* **86** 628
[7] Moon H S, Lee L, Kim K and Kim J B 2004 *Appl. Phys. Lett.* **84** 3001
[8] Bell S C, Heywood D M, White J D, Close J D and Scholten R E 2007 *Appl. Phys. Lett.* **90** 171120
[9] Kale Y B, Ray A, D'Souza R, Lawande Q V and Jagatap B N 2010 *Appl. Phys.* B **100** 505
[10] Fullton D J, Shepherd S, Moseley R R, Sinclair B D and Dunn M H 1995 *Phys. Rev.* A **52** 2302
[11] Kale Y B, Ray A, Lawande Q V and Jagatap B N 2011 *Phys. Scr.* **84** 035401
[12] Jin S, Li Y and Xiao M 1995 *Opt. Commun.* **119** 90
[13] Gea-Banacloche J, Li Y, Jin S and Xiao M 1995 *Phys. Rev.* A **51** 576
[14] Moon H S, Lee L and Kim J B 2005 *J. Opt. Soc. Am.* B **22** 2529
[15] Moon H S, Lee L and Kim J B 2008 *Opt. Exp.* **16** 12163
[16] Abel R P, Mohapatra A K, Bason M G, Pritchard J D, Weatherill K J, Raitzsch U and Adams C S 2009 *Appl. Phys. Lett.* **94** 071107
[17] Moon H S 2011 *Opt. Commun.* **284** 1327
[18] Kale Y B, Ray A, Singh N, Lawande Q V and Jagatap B N 2011 *Eur. Phys. J.* D **61** 221
[19] Shepherd S, Fulton D J and Dunn M H 1996 *Phys. Rev.* A **54** 5394
[20] Zhu Y and Wasserlauf T N 1996 *Phys. Rev.* A **54** 3653

[21] Marangos J P 1998 *J. Mod. Opt.* **45** 471
[22] Li Y, Jin S and Xiao M 1995 *Phys. Rev.* A **51** R1754
[23] Ray A, Ali Md S and Chakrabarti A 2013 *Eur. Phys. J.* D **67** 78
[24] Noh Heung R and Moon H S 2012 *Phys. Rev.* A **85** 033817
[25] Udem T, Reichert J, Holzwarth R and Hänsch T W 1999 *Phys. Rev. Lett.* **82** 3568
[26] Barnes J A *et al* 1971 *IEEE Trans. Instrum. Meas.* **IM-20** 105
[27] Rutman J and Walls F L 1991 *Proc. IEEE* **79** 952
[28] Ray A 2008 *Can. J. Phys.* **86** 351
[29] Brown A W and Xiao M 2004 *Phys. Rev.* A **70** 053830